(Preprint) AAS 22-063

# END-TO-END PERFORMANCE OPTIMIZATION OF A CREWED LUNAR LANDING MISSION STAGED FROM A NEAR RECTILINEAR HALO ORBIT

**Bharat Mahajan[*], Gerald L. Condon[†]**

A crewed lunar landing mission staged from a Near Rectilinear Halo Orbit (NRHO) presents a unique set of challenges not considered before for the Apollo-type direct missions. The NRHO does not have a fixed orbital plane and its period also changes with time, due to which the mission performance is very sensitive to the timing and location of the NRHO departure and arrival burns for a near-polar surface landing site. For such type of mission staged from the NRHO, an end-to-end optimization approach for the entire mission, from the NRHO departure to surface landing and from surface lift-off to the NRHO insertion, is well-suited for extracting the maximum performance out of this design. In this paper, an integrated approach for performing end-to-end optimization of a NRHO-staged crewed lunar landing mission is proposed that optimizes the in-space and powered flight segments simultaneously using Copernicus trajectory optimization tool. Copernicus is augmented with analytical approximations for the in-space, powered descent, and powered ascent segments in this work to improve the convergence of its multiple-shooting based direct optimization method. New analytical solutions are derived for the different phases of the powered flight segments by solving associated guidance problems. These analytical solutions act as initial guesses for starting the numerical optimization of the integrated mission in Copernicus. An example lunar landing mission is simulated to validate the proposed end-to-end optimization approach and the results are compared with the conventional patched trajectory approach.

## INTRODUCTION

The accelerated development by National Aeronautics and Space Administration (NASA) towards returning humans to the lunar surface has resulted in a concentrated re-focus on design and optimization of trajectories for crewed lunar missions. Similar to the Apollo program's manned lunar landing series, the Artemis program leads the effort to, again, place U.S. astronauts on the lunar surface and with it, the associated wide range of technical development necessary to accomplish such an undertaking. To date, the Artemis program focuses on a Concept of Operations (ConOps) that uses a Gateway station as a staging vehicle in a Near Rectilinear Halo Orbit (NRHO) around the Moon for a series of missions to surface landing sites near the lunar South Pole.[1] However, there is also a possibility for the earlier missions to be carried out by stationing Orion in the NRHO if those missions occur before Gateway is placed in the NRHO. The Apollo experience provides today's

[*]Design Engineer/Analyst, Odyssey Space Research LLC, Houston, TX-77058. Adjunct Asst. Professor, Dept. of Aerospace Engineering, Texas A&M University, College Station, TX, 77843. Presently at Flight Mechanics and Trajectory Design Branch, NASA-Johnson Space Center, Houston, TX-77058.

[†]Senior Aerospace Engineer, Flight Mechanics and Trajectory Design Branch, NASA-Johnson Space Center, Houston, TX, 77058.

mission designers with a plethora of useful data, information, lessons learned, and flight operations philosophy. However, there remains an abundance of new considerations specific to these ConOps. Beyond the typical mission design issues associated with a lunar surface landing, the NRHO-staged missions present a unique set of challenges not considered before for the manned missions. This is due, in part, to the fact that the reference NRHO, selected for the Artemis program, is a highly elliptic orbit with perilune over the lunar North Pole that experiences primary gravitational effects from Earth and the Moon as well as secondary effects from the Sun and other bodies.[2] This staging orbit does not have a fixed orbital plane and its period also varies because it is a quasi-periodic orbit. As a result, the mission performance is sensitive to its epoch as well as timing and location of the NRHO departure and arrival burns that occur at the two terminal ends of the mission. The landing site coordinates and lunar surface stay duration also affect the performance of transfer trajectories between the NRHO and the landing site, which in turn affects the mission performance. Therefore, for these kind of lunar missions that are staged from a NRHO type of orbit, an end-to-end optimization approach for the entire mission is well-suited for extracting the maximum performance out of the given mission ConOps. Additionally, this integrated approach provides the capability of modifying the nominal trajectories belonging to one part of the mission for improving the abort (or even nominal) performance of another more critical part. In a typical patched trajectory approach, this latter capability requires multiple design iterations often between different teams if these parts of the mission are optimized separately using different tools.

In NASA's planned lunar missions under Artemis program, the lunar landing vehicle separates from the staging vehicle in the NRHO before starting the lunar mission and, after lunar surface operations, returns back to the same NRHO and docks with the staging vehicle. The current mission design uses in-space coast transfer trajectories separated by relatively short-duration burns and longer-duration powered descent and ascent flight segments for moving crew and supplies between the NRHO and lunar surface.[1] The two types of trajectory segments, namely in-space and powered flight, are typically designed and optimized separately using different methodologies and simulation tools. The in-space transfer trajectories are computed first and their terminal states are used to initialize the powered descent segment and provide targets for the powered ascent segment. It is expected that the performance and operational constraints of the in-space segments of the mission have an impact on that of the powered flight segments and vice-versa. Therefore, the end-to-end optimization of the entire mission including the in-space and powered flight segments, has the potential to maximize the performance gain out of this mission design while still satisfying all the mission-specific constraints. This integrated approach also avoids the possibility of any discontinuity in the trajectory solution, which is a possibility in the patched approach with separately optimized in-space and powered-flight segments.

Multiple approaches exist in the literature for end-to-end trajectory optimization and these typically fall into the two types. In the first type, specialized tools suitable for optimizing either in-space or powered-flight segments are interfaced with each other and run simultaneously using an outer optimization loop to form a framework for end-to-end optimization of the entire mission.[3,4] This versatile approach, while capable of handling many different types of missions, may require significant development effort in interfacing the different optimization tools. Additionally, this approach with multiple tools communicating with each other during every optimization iteration, may exhibit slow run times. The second type of approach fixes the slow run time limitation of the first one by generating response surfaces for one or more flight segments, which capture all the solutions for that segment corresponding to variations in the selected list of parameters. These response surfaces

in the form of pre-generated data set, can be interpolated by the primary optimization tool that performs end-to-end optimization of the entire mission. This approach, while providing faster runs, often requires generating large data sets in advance. The size of these data sets increases exponentially with the number of design parameters and, with it, the order of multi-dimensional interpolation used to keep the errors small. Alternatively, a small set of parameters could be used to decrease the size of the data sets, but this could compromise the optimality of the computed trajectory solution because of more limited optimization controls available to the optimizer.

NASA's POST2 simulation tool[3,5] is primarily used for optimizing atmospheric ascent and entry trajectories including that of SLS and Orion, whereas the Copernicus tool* is typically used for design and optimization of the in-space trajectories. Lack of atmosphere on the Moon simplifies the dynamic models for the powered descent and ascent segments and opens up the possibility of optimizing the entire lunar mission including powered flight segments in Copernicus. This approach provides a unified implementation of the entire mission in a single tool and is also well suited for performing end-to-end performance optimization. Compared to the previous approaches[3,4] considered in the literature for end-to-end optimization, this approach is fast and does not require interfacing different simulation tools through plugin functionality or commercial third-party tools. In the present paper, Copernicus is used for end-to-end performance optimization of an example NRHO-staged crewed lunar landing mission.

Copernicus is a generalized tool for design and optimization of trajectories that uses multiple-shooting based direct method for the transcribing a continuous trajectory optimization problem into a constrained nonlinear programming problem.[6] The transcribed problem can be solved using many nonlinear optimizers available in Copernicus including SNOPT†. Multiple-shooting based optimization methods have generally high sensitivity to the initial conditions compared to the collocation-based methods. The former type of optimization algorithms have small radius of convergence especially for a large constrained optimization problem with multiple time scales existing in the dynamics. The end-to-end optimization of the NRHO-staged lunar landing mission is one such example of the optimization problem. To overcome the small radius of convergence issue in the present work, the numerical optimization capability of Copernicus is augmented with an initial guess generator that provides close approximations for the in-space and powered flight segments to the numerical optimizer. These medium-fidelity analytical solutions provide warm start for the subsequent numerical optimization in Copernicus using its SNOPT solver. The final trajectory solution represents a refined solution optimized in a high-fidelity force model. The major focus of the present work is on developing analytical solutions for the lunar powered descent and ascent trajectories as well as their integration with Copernicus' implementation of the in-space and powered flight segments for performing end-to-end optimization of the NRHO-staged lunar landing missions.

This paper is divided into six sections. The next section briefly discusses the design of the in-space trajectories of an example NRHO-staged lunar landing mission considered in this paper. In the following two sections, analytical solutions for the lunar powered descent and ascent trajectories are derived. The method for integrating these analytical solutions with Copernicus to form a tool for end-to-end optimization of the entire mission is discussed next. Simulation results for the example mission are also presented in this section followed by conclusions.

*https://www.nasa.gov/centers/johnson/copernicus/index.html
†https://web.stanford.edu/group/SOL/snopt.htm

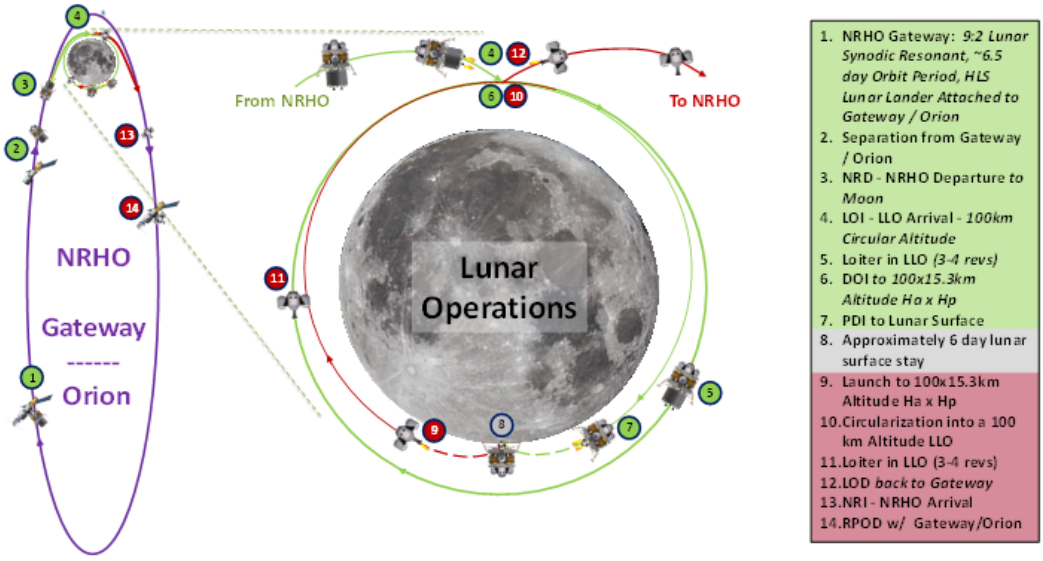


**Figure 1. Potential sequence of events in the Crewed Lunar Landing Mission staged from the NRHO.[1]**

## IN-SPACE TRAJECTORY DESIGN FOR THE LUNAR MISSION

The current design for NASA's planned lunar landing missions uses either a Gateway station or Orion as a staging vehicle in a $9:2$-resonant southern $L_2$ NRHO with the average perilune radius of 3366 km over the lunar North Pole.[2] The mission trajectories include: a transfer from the NRHO to a low lunar orbit (LLO) with a 100 km altitude, a minimum 3-revolution coast in LLO for navigation updates, an elliptical transfer orbit for descent with an apolune of 100 km and a perilune of 15.24 km altitudes, powered descent and powered ascent segments, coast in an elliptical transfer orbit for ascent with a perilune of 15.24 km and an apolune of 100 km altitudes after main engine cutoff (MECO), a post-circularization burn LLO coast of at least 3 revolutions, and a LLO to NRHO transfer. The Powered Descent Initiation (PDI) during descent and Main Engine CutOff (MECO) during ascent occur near the perilune of the elliptical transfer descent and ascent orbits, respectively. A two-stage vehicle configuration consisting of a Descent Element (DE) and an Ascent Element (AE) is assumed in this work. The use of at least three loiter revs in LLO provides the necessary time for navigation updates and crew preparation as well as flexibility in landing site access with reduced adverse performance impacts for powered descent and ascent.[1] Additionally, the use of the LLO simplifies the integration of the powered descent and ascent flight segments with the in-space trajectories of the mission, which benefits the overall end-to-end mission design and optimization. One potential sequence of events in NASA's planned lunar landing missions is shown in Fig. 1.[1] In the present paper, the same mission ConOps are used for validating the optimization capability of the proposed end-to-end optimization approach. An analytical tool for generating an initial guess for the in-space trajectories of this mission was developed in the previous work, to help the numerical convergence in Copernicus.[1] The same tool along with the analytical solutions for the powered flight segments (see the next section) is integrated with Copernicus to implement a tool for the end-to-end optimization of the NRHO-staged lunar landing missions.

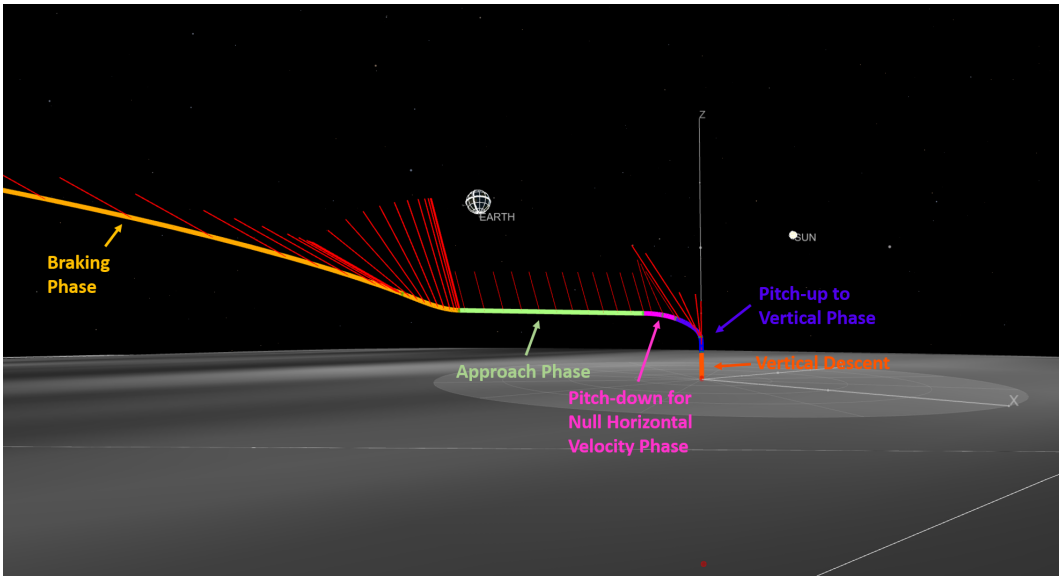


**Figure 2. The powered descent trajectory with multiple phases.**

## ANALYTICAL SOLUTION FOR POWERED DESCENT

In this section, an analytical approach for designing each phase of the lunar powered descent trajectory is developed. The analytical equations derived in this section are used to construct initial guesses for starting the numerical optimization of the powered descent trajectory segments in Copernicus. It is, however, noted that these solutions may also be useful for developing guidance algorithms for onboard implementation in case of lunar powered descent (and ascent in the following section).

In the example lunar mission design, as discussed in the previous section, the combined DE+AE stack performs PDI before the perilune of the elliptical descent orbit is reached. A typical lunar powered descent trajectory is divided into multiple phases based on different constraints that each phase must satisfy for a viable descent trajectory. In the present work, the powered descent is divided into five phases and each phase is shaped according to the specific mission requirements. These five phases are braking phase (BP), approach phase (AP), pitch-down for null horizontal velocity (BN) phase, and terminal descent (TD) as shown in Fig. 2. For finding the analytical solution for each of these phases, the general equation of motion valid for a thrusting vehicle flying close to the surface of a rotating planet may be used. The kinematic equations for such a vehicle are[7]

$$\dot{r} = V \sin\gamma, \tag{1}$$

$$\dot{\theta} = \frac{V \cos\gamma \cos\psi}{r \cos\phi}, \tag{2}$$

$$\dot{\phi} = \frac{V \cos\gamma \sin\psi}{r}, \tag{3}$$

where $V$ is the velocity of the vehicle in the planet-fixed frame, $\gamma$ is the flight-path angle, $\psi$ is the azimuth angle of the velocity vector from the East direction, and $\theta$ and $\phi$ are the longitude and latitude of the vehicle, respectively. The Kinetic equations in the planet-fixed frame generally include

the Coriolis and centripetal acceleration terms in addition to the thrust and aerodynamic forces. For a celestial body with no atmosphere such as the Moon, the aerodynamic forces can be ignored. Additionally, if the rotational velocity of the planet and flight time duration is sufficiently small, then Coriolis terms can also be ignored from the Kinetic equations and $V$ can be approximated as the inertial velocity magnitude for computing a medium-fidelity solution. The resulting simplified kinetic equations for powered flight of the vehicle are (see Section 3 in Reference 7)

$$\dot{V} = a_T \cos\zeta \cos\epsilon - g \sin\gamma, \tag{4}$$

$$V\dot{\gamma} = a_T \cos\zeta \sin\epsilon - g \cos\gamma + \frac{V^2}{r} \cos\gamma, \tag{5}$$

$$V\dot{\psi} = -a_T \frac{\sin\zeta}{\cos\gamma} - \frac{V^2}{r} \cos\gamma \cos\psi \tan\phi, \tag{6}$$

$$\dot{m} = -\frac{T}{g_0 I_{sp}}, \tag{7}$$

where

$$a_T = \frac{T}{m},$$

$m$ is the total vehicle mass, $g_0$ is standard gravity, $T$ is thrust magnitude, $\epsilon$ is the angle made if $\boldsymbol{V}$ is rotated about $\boldsymbol{V} \times \boldsymbol{r}$ vector to align it with the projection of thrust direction on $(\boldsymbol{r}, \boldsymbol{V})$ plane, and $\zeta$ is the angle made by the thrust projection on $(\boldsymbol{V}, \boldsymbol{h})$ plane if it is rotated about the $\boldsymbol{V} \times \boldsymbol{h}$ vector to align it with $\boldsymbol{V}$. The boldface notation is used to represent vector quantities in this work. If no yaw steering is used during powered descent (and ascent) then $\zeta = 0$ and as a consequence, the Kinetic and mass equations simplify to

$$\dot{V} = a_T \cos\epsilon - g \sin\gamma, \tag{8}$$

$$V\dot{\gamma} = a_T \sin\epsilon - g \cos\gamma + \frac{V^2}{r} \cos\gamma, \tag{9}$$

$$\dot{\psi} = -\frac{V}{r} \cos\gamma \cos\psi \tan\phi, \tag{10}$$

$$\dot{m} = -\frac{T}{g_0 I_{sp}}. \tag{11}$$

In the present work, $\dot{\psi}$ is considered sufficiently small that the powered descent and ascent trajectories can be safely assumed to lie in a fixed vertical plane with no out-of-plane motion. The thrust acceleration is assumed to be constant for deriving analytical solutions for the powered descent. With this assumption, the variation of mass during any flight phase can be easily determined using

$$m_f = m_0 \exp\left(-\frac{a_T}{g_0 I_{sp}}(t_f - t_0)\right), \tag{12}$$

where $t$ is time and the subscripts $0$ and $f$ denote quantities at the initial and final time, respectively. If, instead, constant thrust is used during powered flight, then mass varies linearly over time.

**Braking Phase using Gravity-Turn Guidance**

In this subsection, the gravity-turn guidance solution is used to provide an analytical solution for the braking phase of the powered descent trajectory. In gravity-turn guidance, thrust is applied in opposite direction to that of the instantaneous velocity vector, i.e., $\epsilon = 180^\circ$ in Kinetic equations. It is known that the pure gravity-turn guidance produces a descent trajectory that terminates with vertical landing.[8] However, in the present work, the gravity-turn guidance is terminated before the start of the approach phase for accommodating specific goals for crewed mission as discussed in the next subsection. For computing analytical solution for the gravity-turn guidance, it is assumed that the thrust acceleration is constant and the altitude ($h$) is small compared to $R_0$, i.e., $r = R_0(1 + h/R_0) \approx R_0$, where $R_0$ is the radius of the Moon. Then, the resulting Kinetic equations are

$$\dot{V} = -a_T - g\sin\gamma, \tag{13}$$

$$V\dot{\gamma} = \left(\frac{V^2}{R_0} - g\right)\cos\gamma. \tag{14}$$

These equations can be divided to obtain a separable differential equation as

$$\frac{1}{V}\left(1 - \frac{V^2}{gR_0}\right)\mathrm{d}V = \frac{(a_T/g) + \sin\gamma}{\cos\gamma}\mathrm{d}\gamma, \tag{15}$$

that can be integrated to yield

$$\ln\frac{V_f}{V_0} - \frac{\rho^2}{2}\left(\left(\frac{V_f}{V_0}\right)^2 - 1\right) = \ln\frac{G(N,\gamma_f)}{G(N,\gamma_0)}, \tag{16}$$

where

$$\rho = \frac{V_0}{V_c}, \tag{17}$$

$$G(N,\gamma) = \frac{(\sec\gamma + \tan\gamma)^N}{\cos\gamma}, \tag{18}$$

$V_c = \sqrt{gR_0}$ is the circular orbit speed at zero altitude, and $N = a_T/g$ is the thrust-to-lunar-weight ratio. If $V_0$ is insignificant compared to $V_c$, then $\rho$ can be approximated as zero. In that case, the solution for the velocity magnitude is simply

$$V_f = V_0\frac{G(N,\gamma_f)}{G(N,\gamma_0)}. \tag{19}$$

For $\rho \neq 0$, Eq. (16) may be written as

$$W\exp(W) = -\rho^2\exp(-\rho^2)\frac{G^2(N,\gamma_f)}{G^2(N,\gamma_0)}, \tag{20}$$

where

$$W \equiv -\rho^2 \left(\frac{V_f}{V_0}\right)^2.$$

The preceding equation can be solved for $W$ using the LambertW function, which is an inverse function of $f(W) = W\exp(W)$. Therefore, in terms of this function, the solution to the preceding equation may be written as:[9]

$$V_f = \frac{V_0}{\rho}\sqrt{-\text{LambertW}\left(-\rho^2\exp(-\rho^2)\frac{G^2(N,\gamma_f)}{G^2(N,\gamma_0)}\right)}. \tag{21}$$

The LambertW($x$) returns real values for $x \geq -1/e$, where $e$ is Euler's number. For starting descent from near-circular orbits, $\rho$ is closer to unity, $\gamma_0 \approx 0$, and $\gamma_f < 0$. For these conditions, it can be verified that $G(N,\gamma_0) = 1$ and $G(N,\gamma_f)$ lies between 0 and 1. Therefore, the argument of the LambdaW function in the preceding equation is greater than $-1/e$ and thus, a real value for $V_f$ can be obtained from the preceding equation. For the calculation of final time, Eq. (14) is used as shown below:

$$\int_{\gamma_0}^{\gamma_f} \frac{V}{\left(\frac{V^2}{R_0} - g\right)\cos\gamma}\,\mathrm{d}\gamma = (t_f - t_0). \tag{22}$$

This quadrature can be numerically solved; however, an analytical solution exists if the contribution of the centripetal acceleration term, i.e., $V^2/R_0$ is ignored in the equations of motion (EOM). The result is

$$\frac{V_0}{(N^2-1)G(N,\gamma_0)}\left((N-\sin\gamma_f)G(N,\gamma) - (N-\sin\gamma_0)G(N,\gamma_0)\right) = -g\,(t_f - t_0), \tag{23}$$

which is derived by substituting Eq. (19) in Eq. (14), ignoring $V^2/R_0$ term, and then carrying out the integration.

This gravity-turn analytical solution for the braking phase is compared against numerically propagated trajectory in Copernicus with spherical-Moon gravity model for verification. As an example, consider a vehicle with constant thrust-to-weight ratio as $1.70$, initial velocity and flight-path angle as $1.69$ km/s and $0.02^\circ$, respectively. If targeted flight-path angle is known, then the final velocity analytically calculated from Eq. (21) is $0.89$ km/s. The time of flight is calculated from Eq. (22) by using numerical quadrature and the result is $289$ s. The results for a numerically propagated trajectory in Copernicus for the same initial conditions are found to be off by less than $1\%$ and $4\%$ for the final velocity and time of flight, respectively. A better use case of this analytical solution is to calculate the time of flight required for reducing the initial velocity to a desired final value. If this desired final velocity is selected as $0.89$ km/s then Eq. (21) can be solved for the final flight-path angle using any nonlinear root finding solver (e.g., Newton's method). Subsequently, the final time can be calculated from Eq. (22) by numerical quadrature as before. The comparison with numerically-propagated results in Copernicus shows less than $3\%$ error for the final-time calculated using this analytical solution.

**Approach Phase**

After completion of the braking phase, the descent trajectory enters the approach phase. The trajectory during this phase is shaped to have a constant glide slope so that the crew can have direct line-of-sight visibility to the landing site. This allows the crew to make final decision on whether continue the descent, divert to a different landing site or even abort the descent completely to get back to the LLO or NRHO in case of a contingency. The duration of the approach phase is kept above a minimum value to allow crew to have sufficient time for making these crucial decisions. After the braking phase, the velocity is sufficiently small and therefore, $V^2/r$ term becomes insignificant in the EOM. If flight-path angle is assumed constant during the approach phase, then Eqs. (8)-(9) for this phase may be written as

$$a_T \sin\epsilon = g\cos\gamma, \tag{24}$$

$$a_T \cos\epsilon = \dot{V} + g\sin\gamma. \tag{25}$$

Squaring these equations and adding, yields

$$a_T^2 - g^2\cos^2\gamma - (\dot{V} + g\sin\gamma)^2 = 0, \tag{26}$$

which can be solved for the final velocity assuming constant $a_T$ as

$$V_f = V_0 + \left(-g\sin\gamma \pm \sqrt{a_T^2 - g^2\cos^2\gamma}\right)(t_f - t_0). \tag{27}$$

The approach phase guidance command for thrust direction that ensures constant glide slope (or flight-path angle) is found by dividing Eq. (24) by Eq. (25) and using Eq. (27):

$$\epsilon = \tan^{-1}\left(\frac{g\cos\gamma}{\pm\sqrt{a_T^2 - g^2\cos^2\gamma}}\right). \tag{28}$$

It is noted that in order to guarantee real solutions for $\epsilon$ using this result, $a_T$ must be greater than $g$. Two solutions of $\epsilon$ will result from the preceding equation corresponding to the two signs of the square-root term. If the positive sign is considered, $\epsilon$ will lie in the first quadrant and as a result, thrust acceleration will work to increase the velocity magnitude. The negative sign is chosen here so that $90^\circ < \epsilon < 180^\circ$ and velocity magnitude of the landing vehicle (or DE+AE stack) decreases during the approach phase.

The landing site visibility requirement is not taken into account so far for deriving the expression for the thrust direction during the approach phase. Attitude of the descent vehicle directly affects the landing site visibility to the crew and thrust direction determines the yaw and pitch angle of the vehicle (assuming the thrust direction remains fixed in the spacecraft's body frame). Figure 3 shows the geometry of the landing site visibility problem during the approach phase. The angle between the thrust direction and line of sight to the landing site as shown in this figure is referred to as the look angle ($\lambda$). It is apparent from this geometry that landing site will not be visible to the crew if $\lambda = 0$, i.e., the thrust direction is aligned with the line-of-sight vector to the landing site. Owing to

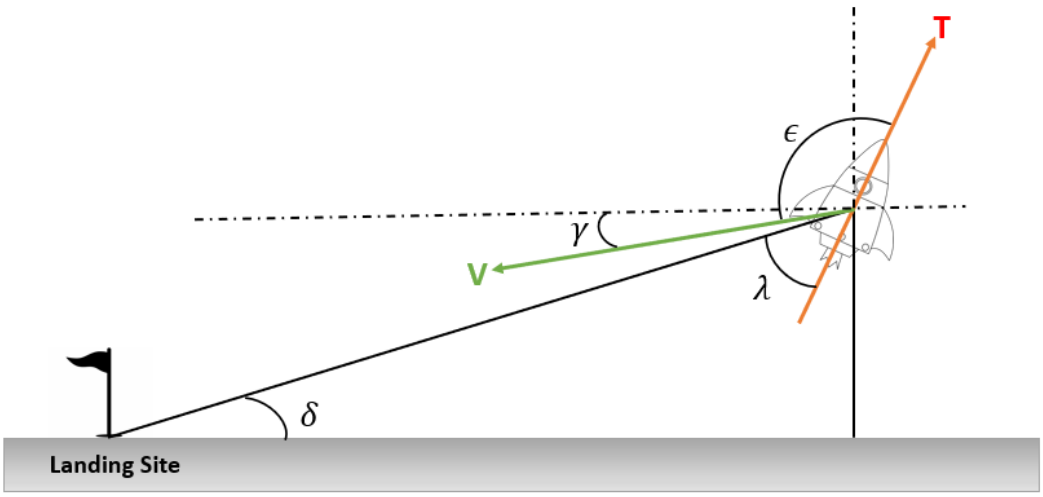


**Figure 3. Look angle geometry. $V$ and $T$ represent velocity and thrust directions, respectively.**

the spacecraft size and shape, there is a minimum non-zero value of $\lambda$ below which the landing site will not be visible. During the approach phase, the trajectory must be shaped such that the actual $\lambda$ remains above this minimum value. From Fig. 3, $\lambda$ can be related to the spacecraft declination with respect to the landing site, $\gamma$, and $\epsilon$ using

$$\lambda = 90^\circ - \delta - (\epsilon - 90^\circ + \gamma), \tag{29}$$

$$= 180^\circ - \delta - \epsilon - \gamma. \tag{30}$$

Then, a simple guidance command for $\epsilon$ may be derived for maintaining a preferred value for $\lambda$ as follows:

$$\epsilon = 180^\circ - \delta - \lambda - \gamma, \tag{31}$$

$$\dot{\epsilon} = \dot{\delta} - \dot{\lambda} - \dot{\gamma}. \tag{32}$$

If $\epsilon$ and $\gamma$ are kept constant during the approach phase, $\lambda$ will generally vary unless the spacecraft approaches the landing site along the line-of-sight vector. For the short duration of the approach phase if the boundary conditions can be found such that $\lambda$ remains above the minimum value then the constant-flight path angle guidance command from Eq. (28) along with the constraint from Eq. (31) can be used for generating an initial guess for the approach trajectory. Equating these two equations for $\epsilon$ yields

$$\frac{g\cos\gamma}{\pm\sqrt{a_T^2 - g^2\cos^2\gamma}} = -\tan(\delta + \lambda + \gamma). \tag{33}$$

This may be further simplified to obtain an expression for the required $a_T$ as

$$a_T = g\sqrt{\frac{\cos^2\gamma}{\sin^2(\delta+\lambda+\gamma)}}. \tag{34}$$

For the approach phase solution to exist with constant $a_T$ and $\gamma$, the quantity $(\delta + \lambda)$ must be constant or $\dot{\lambda} = \dot{\delta}$. For such solutions, $\epsilon$ and $\dot{V}$ will also be constant as already seen in the preceding results and an expression for the variation of $\lambda$ along this trajectory solution may be derived. If $x$ and $y$ represent downrange and altitude of the landing vehicle during the approach phase, then

$$\begin{aligned}
\dot{\delta} &= \frac{\mathrm{d}}{\mathrm{d}t}\tan^{-1}(y/x), \\
&= \frac{V}{x^2+y^2}\left(x\sin\gamma - y\cos\gamma\right), \\
&= \frac{V}{\sqrt{x^2+y^2}}\sin(\gamma-\delta).
\end{aligned} \tag{35}$$

In this equation, $V$ varies linearly with time and $x$ and $y$ are quadratic functions of time. Therefore, this equation may be solved by separation of variables to obtain an expression for $\delta$ (and $\lambda$) as a function of time. If the velocity vector during the approach phase lies above the line-of-sight vector to the landing site as shown in Fig. 3, then $\delta$ will increase with time and as a result, $\lambda$ will decrease with the same rate as that of $\delta$. Therefore, a higher than minimum desired value of $\lambda$ should be chosen at the start of the approach phase. Consider a case in which at the end of the braking phase, the velocity, flight-path angle, and $\delta$ angle w.r.t. the landing site are $-15.07^\circ$, $0.041$ km/s, and $26.12^\circ$, respectively. These values may be considered as the initial conditions for the approach phase. If the desired look angle at the start of the approach phase is $52.3^\circ$, then required $\epsilon$ and $a_T$ values are $116.62^\circ$ and $1.754$ m/s$^2$ as computed using Eqs. (28) and (34), respectively. If approach phase time duration is $45$ s, then at the end of the approach phase $\delta$ is $53.3^\circ$ and as a result, the final value of $\lambda$ from Eq. (31) turns out to be $25.2^\circ$. These results are verified to have less than $1\%$ error when compared against the numerically propagated approach phase trajectory in Copernicus with the spherical-Moon gravity model.

It is remarked that another analytical solution for the approach phase is also possible in which $\lambda$ is kept constant. In this case, the landing site will always lie in the same direction for the crew in the landing vehicle, which may have an operational advantage for the crew. For this case, $\dot{\epsilon} = \dot{\delta} - \dot{\gamma}$. If $\epsilon$ is kept constant then $\gamma$ must be varied to account for the variation in $\delta$ for maintaining a constant $\lambda$. By keeping $\epsilon$ constant, the EOM can still be separated and analytically solved for the velocity as seen in the velocity-turn solution derived in the sequel.

**Velocity-Turn Guidance for Pitch-up/down Phase**

The pitch of the descent vehicle is first increased and then decreased to $-90^\circ$ after the completion of the approach phase as shown by the thrust direction in Fig. 2. In other words, the velocity vector is rotated about the horizontal axis after the approach phase until it is aligned with the local vertical axis just before the terminal descent starts. In this subsection, a new analytical solution is derived for solving the guidance problem in which the velocity vector of a thrusting vehicle needs to be rotated about the local horizontal axis to attain a desired flight-path angle and is referred to as velocity-turn guidance in this paper. One way to rotate the velocity vector is by applying thrust normal to the

instantaneous velocity vector.[10] However, the EOM for this problem can be solved analytically in a more generalized form with thrust direction kept constant with respect to the velocity as seen in the sequel. The results may be then simplified for the special case of thrust being exactly normal to the velocity. For solving the velocity-turn guidance problem, the kinetic EOM after ignoring the centripetal acceleration terms may be written as

$$\dot{V} = a_T \cos\epsilon - g\sin\gamma, \tag{36}$$

$$V\dot{\gamma} = a_T \sin\epsilon - g\cos\gamma, \tag{37}$$

where $\epsilon$ and $a_T$ are considered constant. Dividing the two equations and separating the variables yield

$$\frac{\mathrm{d}V}{V} = \frac{N\cos\epsilon - \sin\gamma}{N\sin\epsilon - \cos\gamma}\,\mathrm{d}\gamma, \tag{38}$$

where $N\,(= a_T/g)$ is the thrust-to-weight ratio. Integrating this equation yields

$$\ln\frac{V_f}{V_0} = \ln\frac{P-\cos\gamma_0}{P-\cos\gamma_f} + \frac{2Q}{\sqrt{P^2-1}}\left[\tan^{-1}\left(\frac{P+1}{\sqrt{P^2-1}}\tan\frac{\gamma_f}{2}\right) - \tan^{-1}\left(\frac{P+1}{\sqrt{P^2-1}}\tan\frac{\gamma_0}{2}\right)\right], \tag{39}$$

where $P = N\sin\epsilon$ and $Q = N\cos\epsilon$. Since

$$\tan^{-1}x = \frac{i}{2}\ln\frac{1-ix}{1+ix}, \tag{40}$$

the preceding result may be written as

$$\frac{V_f}{V_0} = \frac{P-\cos\gamma_0}{P-\cos\gamma_f}\left[\frac{\left(1-\bar{P}\tan\frac{\gamma_f}{2}\right)\left(1+\bar{P}\tan\frac{\gamma_0}{2}\right)}{\left(1+\bar{P}\tan\frac{\gamma_f}{2}\right)\left(1-\bar{P}\tan\frac{\gamma_0}{2}\right)}\right]^{\frac{Q}{\sqrt{1-P^2}}}, \tag{41}$$

where

$$\bar{P} = \frac{1+P}{\sqrt{1-P^2}}.$$

It can be verified that this equation produces real solutions for $V_f$ if $P < 1$ because in that case, the term

$$\frac{1-\bar{P}\tan\frac{\gamma}{2}}{1+\bar{P}\tan\frac{\gamma}{2}} \tag{42}$$

can be expressed in the complex exponential form $\exp(i\theta)$, where $\theta$ is a function of $\gamma$ and $\epsilon$. Additionally, this result reduces to that of the classic gravity-turn guidance solution (see Eq. (19)) if

$\epsilon = 180^\circ$. From Eqs. (37) and (41), the following equation is obtained that can be used to compute the time required for changing the flight-path angle from $\gamma_0$ to $\gamma_f$:

$$\int_{\gamma_0}^{\gamma_f} \frac{P - \cos\gamma_0}{(P - \cos\gamma)^2} \left[ \frac{\left(1 - \bar{P}\tan\frac{\gamma}{2}\right)\left(1 + \bar{P}\tan\frac{\gamma_0}{2}\right)}{\left(1 + \bar{P}\tan\frac{\gamma}{2}\right)\left(1 - \bar{P}\tan\frac{\gamma_0}{2}\right)} \right]^{\frac{Q}{\sqrt{1-P^2}}} \mathrm{d}\gamma = g(t_f - t_0), \tag{43}$$

where the unknowns $P$ and $Q$ can be selected to obtain a desired value for $V_f$ from Eq. (41). This equation can be solved by numerical quadrature to obtain $t_f$. However, an analytical solution exists if the thrust is always assumed to be in a normal direction to that of the velocity, i.e., $\epsilon = \pm 90^\circ$. In this case, the preceding equation simplifies to

$$\int_{\gamma_0}^{\gamma_f} \frac{\pm N - \cos\gamma_0}{(\pm N - \cos\gamma)^2} \mathrm{d}\gamma = g(t_f - t_0), \tag{44}$$

where the $+$ and $-$ signs apply to $\epsilon = 90^\circ$ and $\epsilon = -90^\circ$ cases, respectively. Carrying out the integration yields

$$V_f \sin(\gamma_f) - V_0 \sin(\gamma_0) + \frac{2NV_0(\pm N - \cos\gamma_0)}{\sqrt{N^2 - 1}} \left( \tan^{-1}(\bar{N}\tan\gamma_f/2) - \tan^{-1}(\bar{N}\tan\gamma_0/2) \right) = g(N^2 - 1)(t_f - t_0), \tag{45}$$

where

$$\bar{N} = \frac{N \pm 1}{\sqrt{N^2 - 1}}$$

It is noted that this equation is singular for $N = 1$ case, however, an equivalent equation valid for $N = 1$ case can easily be found by letting $a_T = g$ in the EOM and following the same procedure.

For verification, consider a descent vehicle that needs to turn its velocity vector up to set up the initial conditions for the next phase of the descent trajectory. This scenario may be needed near the end of the braking phase to set up the desired velocity direction during the approach phase. If $N = 2.84$ and thrust is normal to the velocity vector, i.e., $\epsilon = 90^\circ$, along with the desired boundary conditions as $V_0 = 68.8$ m/s, $\gamma_0 = -19^\circ$, $\gamma_f = -1.1^\circ$, then from Eq. (41), $V_f$ is 70.8 m/s and the final time from Eq. (45) is 7.3 s. These results are found to be in close agreement with the numerical propagated results in Copernicus. It is noted that if a desired value of $V_f$ is known, then Eq. (41) can be solved for thrust direction ($\epsilon$) using any numerical root solver. Consider such a case in which velocity vector needs to be rotated down from $\gamma_0 = -22.98^\circ$ to $\gamma_f = -79.35^\circ$ with the fixed initial and final velocity magnitudes as 20.2 m/s and 8.8 m/s, respectively. If $N$ is chosen as 1.54, then root solving Eq. (41) for $\epsilon$ gives $-168.4^\circ$ and evaluating Eq. (43) using numerical quadrature yields 9.24 s for the time of flight.

**Terminal Descent**

The velocity-turn analytical solution derived in the previous subsection is useful for generating initial guesses for the trajectory segments that connect the approach phase to the terminal descent.

The vehicle descends from a fixed altitude to the surface in a controlled manner during the terminal descent. The vertical velocity of the vehicle is decreased to a sufficiently small value just before the touchdown. For terminal descent, the minimum-$\Delta v$ optimal solution is equivalent to the minimum-time solution. This optimal solution can be shown to be either in the form of full thrust until touchdown or free-fall followed by full thrust until touchdown.[11] This latter solution is not operationally desirable especially for a crewed mission as errors in thrust ignition timing could compromise the soft touchdown requirement. Rather than flying a fuel-optimal solution, the descent rate of the vehicle during terminal descent is typically selected a priori for crewed missions to reduce the vehicle altitude in a fixed time duration and with a small final velocity for a soft touchdown. During the terminal descent, $\gamma = -90^\circ$ and $\epsilon = 180^\circ$, and as a result, the kinematic and kinetic EOM assume the simple form as

$$\dot{V} = g - a_T, \tag{46}$$

$$\dot{r} = -V. \tag{47}$$

These equations can be integrated without any difficulty to obtain

$$V_f - V_0 = (g - a_T)(t_f - t_0), \tag{48}$$

$$r_f - r_0 = -V_0(t_f - t_0) - \frac{1}{2}(g - a_T)(t_f - t_0)^2. \tag{49}$$

If the initial and final altitudes and velocities are specified, then these equations can be used to compute the thrust acceleration and time of flight required for the terminal descent phase.

## ANALYTICAL SOLUTION FOR POWERED ASCENT

Similar to the powered descent, the complete powered ascent trajectory is divided into three phases, namely: vertical lift-off, pitch-over, and ascent to orbit as shown in Fig. 4. The powered ascent trajectory is relatively simpler and has fewer mission constraints compared to the powered descent. The vertical lift-off phase is used to allow the ascent vehicle (or AE) to rapidly gain altitude so as to stay clear of any ridges and mountains when ascending to the orbit. After lift-off, the vehicle is pitched-over in order to rotate the velocity vector and gain the horizontal velocity. In the final phase, the vehicle uses maximum thrust to gain altitude and achieve orbital velocity for injecting into the ascent orbit. To simplify the propulsion system of the ascent vehicle, typically ascent vehicle uses constant maximum thrust for the entirety of the powered ascent. However, in this work it is assumed that the ascent vehicle can throttle its engine to different thrust levels during lift-off, pitch-over, and ascent to orbit phases to minimize the fuel consumption.

### Vertical Lift-Off

The EOM for the vertical lift-off phase are similar to that of the terminal descent with the exception that $\gamma = 90^\circ$ and $\epsilon = 0^\circ$ in this case. That is,

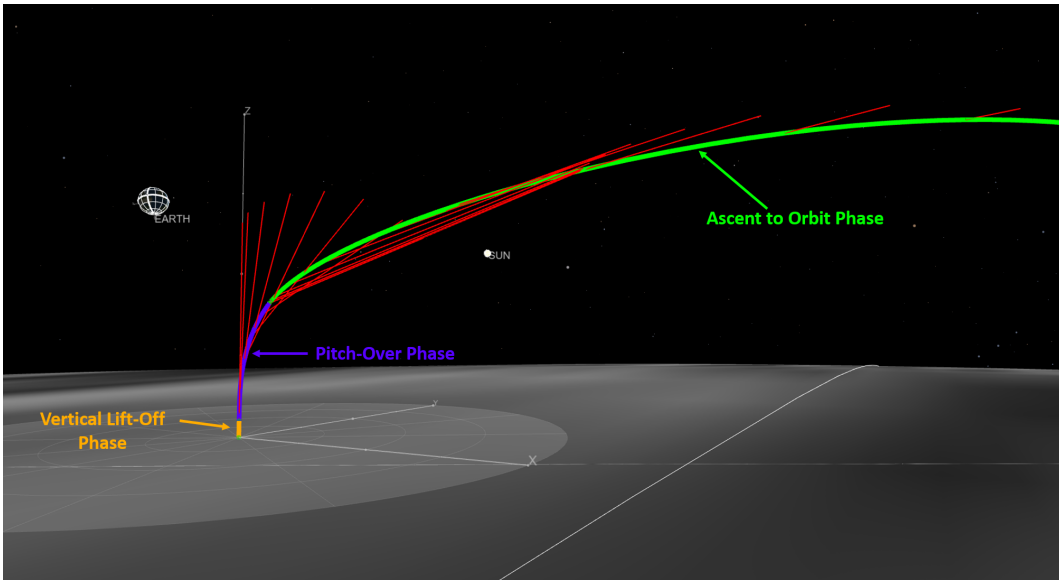


**Figure 4. The powered ascent trajectory with multiple phases.**

$$\dot{m} = -\frac{T}{c}, \tag{50}$$

$$\dot{V} = T/m - g, \tag{51}$$

$$\dot{r} = V, \tag{52}$$

where $c = g_0 I_{sp}$. These equations can be easily integrated if $T$ is assumed constant, to obtain

$$m(t) = m_0 - \frac{T}{c}t, \tag{53}$$

$$V(t) = -c\ln\left(1 - \frac{T}{m_0 c}t\right) - gt, \tag{54}$$

$$r(t) = r_0 - \frac{gt^2}{2} + c\left(t - \left(t - \frac{m_0 c}{T}\right)\ln\left(1 - \frac{T}{m_0 c}t\right)\right), \tag{55}$$

where the initial time is assumed to be 0. If the final time and $T$ are considered free parameters, then the following parameter optimization problem can be formulated to maximize the final mass (payload) for achieving a fixed altitude:

$$\begin{aligned} &\text{Minimize} \quad J(T,t) \\ &\text{subject to} \quad r_f = r_0 - \frac{gt^2}{2} + c\left(t - \left(t - \frac{m_0 c}{T}\right)\ln\left(1 - \frac{T}{m_0 c}t\right)\right), \end{aligned} \tag{56}$$

where

$$J(T,t) = -\left(m_0 - \frac{Tt}{c}\right). \tag{57}$$

$J(T,t)$ is the cost function that needs to be minimized using two free parameters $T$ and $t$ subject to the final altitude constraint. A simple optimizer such as Matlab's *fmincon* is sufficient for this optimization problem. Because the engine's $I_{sp}$ are considered constant in this work, this optimization problem is equivalent to minimizing $\Delta v$ given by

$$\Delta v = c \ln\left(\frac{m_0}{m_0 - Tt/c}\right). \tag{58}$$

If Eq. (56) is solved for the final time to achieve a fixed altitude of 100 m with $I_{sp} = 340$ s for a range of values of $T$ and the corresponding $\Delta v$ values are plotted as in Fig. 5, it is apparent that the optimal thrust value is not the maximum and this is not a minimum-time optimization problem. When optimizing the entire powered ascent trajectory and not just the lift-off segment, the optimal solution for the entire powered ascent typically uses a sub-optimal lift-off solution that has lower final velocity at the conclusion of the lift-off. This is due to the fact that this solution incurs lower cost in the pitch-over phase during which the velocity vector is rotated about the local horizontal axis before starting ascent to the orbit.

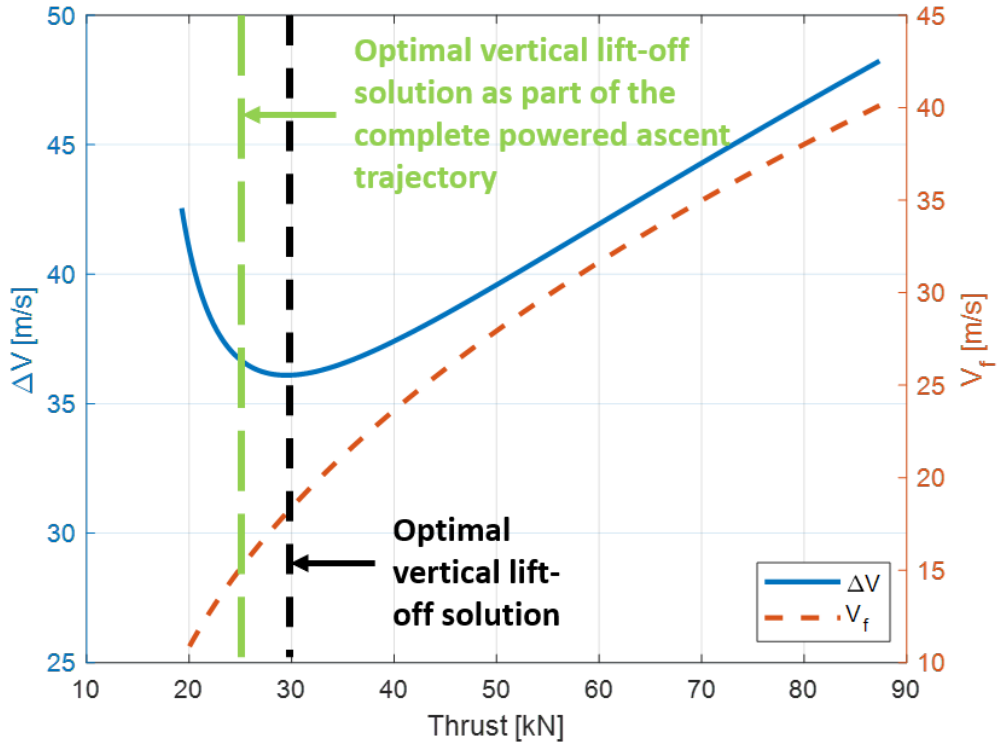


**Figure 5. Cost and final velocity variation of vertical lift-off phase with thrust.**

### Pitch-Over Phase

In the pitch-over phase, the pitch angle of the ascent vehicle is increased to less negative values to gain the horizontal velocity with correct azimuth to insert into the ascent orbit. The velocity-turn guidance equations derived earlier are used to generate close initial guesses for this part of the powered ascent trajectory in the present work.

### Ascent to Orbit Phase

Following the pitch-over phase, the ascent vehicle increases its altitude and velocity both. The gravity-turn guidance solution discussed in the previous section can be used to generate close initial guess for this phase of the powered ascent also. However, the thrust direction during this phase is opposite to that of in the descent gravity-turn equations. Therefore, the guidance equations for this phase differ by a sign. The EOM for the ascent to orbit phase are

$$\dot{V} = a_T - g\sin\gamma, \tag{59}$$

$$V\dot{\gamma} = \left(\frac{V^2}{R_0} - g\right)\cos\gamma. \tag{60}$$

These equations can be integrated in the same way as for the descent gravity-turn solution to obtain

$$V_f = \frac{V_0}{\rho}\sqrt{-\text{LambertW}\left(-\rho^2\exp(-\rho^2)\frac{G^2(N',\gamma_f)}{G^2(N',\gamma_0)}\right)}, \tag{61}$$

where $N' = -a_T/g$. For the calculation of the final time, Eq. (60) is integrated to obtain

$$\int_{\gamma_0}^{\gamma_f} \frac{V}{\left(\frac{V^2}{R_0} - g\right)\cos\gamma}\,\mathrm{d}\gamma = (t_f - t_0), \tag{62}$$

which can be solved using numerical quadrature. Consider an ascent to orbit example with the initial velocity and flight-path angle as $45.1$ m/s and $52.3^\circ$, respectively. If the desired final flight-path angle is $12.4^\circ$, then the final velocity and time of flight are calculated from Eqs. (61) and (62) and are equal to $1254.8$ m/s and $199.8$ s, respectively. These results are verified against numerical propagation in Copernicus with the spherical-Moon gravity model.

## END-TO-END OPTIMIZATION OF THE LUNAR MISSION

In this section, the integrated simulation of the NRHO-staged lunar landing mission in Copernicus for performing end-to-end optimization is described. This integrated simulation includes all the trajectories from the NRHO departure to lunar surface landing and from surface lift-off to the NRHO insertion. The assumed parameters for a two-stage vehicle configuration consisting of DE and AE are given in Table 1. In this simulation, mass of the DE+AE stack is initialized just before the NRD burn for the lunar descent leg of the mission and the AE mass is initialized just before the lunar surface lift-off for the ascent leg. The trajectories of DE and AE are simulated in the three degree-of-freedom (3-DOF) mode and optimized in Copernicus using its multiple-shooting based direct method.[6] This integrated simulation in Copernicus is very sensitive to the initial conditions

**Table 1. Two-Stage Vehicle Configuration**

| Parameter | Value |
|---|---|
| DE Wet Mass | 33146 kg |
| DE Main Propulsion Engine (MPS) Max Thrust | 9.8217 N |
| DE MPS $I_{sp}$ | 340 s |
| DE RCS $I_{sp}$ (only for DOI burn) | 300 s |
| AE Wet Mass | 9121 kg |
| AE Main Propulsion Engine (MPS) Max Thrust | 58800 N |
| AE MPS $I_{sp}$ | 340 s |
| AE RCS $I_{sp}$ (only for LLO circ. burn) | 300 s |

**Table 2. Controls and Constraints for the In-Space Trajectory Segments in Copernicus**

| Controls | Constraints |
|---|---|
| NRD burn vector and time | NRHO-to-LLO transfer time = 12 hr |
| LOI burn vector | Descent and Ascent LLO altitude = 100 km |
| Descent LLO $I$, $\Omega$ | Minimum 3 revs in Descent LLO before DOI |
| DOI burn vector and time | Post-DOI descent orbit perilune altitude = 15.24 km |
| Surface stay duration | Post-MECO ascent orbit perilune altitude = 15.24 km |
| LLO circ. burn vector and time | Perilune of the descent and ascent orbits over the landing site |
| Ascent LLO $I$, $\Omega$ | Minimum 3 revs in Ascent LLO before LOD |
| LOD burn vector and time | LLO-to-NRHO transfer time = 12 hr |
| NRI burn vector | NRD-to-NRI mission time $<$ NRHO period+1.5 day |

owing to the type of optimization method used and multiple time scales present in the problem. The analytical results derived in the previous sections for computing approximations for the in-space, powered descent, and powered ascent segments, are used to seed this integrated simulation with close initial guesses for each trajectory segment. These initial guesses are directly inserted into the Copernicus' input deck files before starting the end-to-end optimization. This strategy improves the numerical convergence of Copernicus' direct optimization method and also reduces the number of iterations its SNOPT gradient-based optimizer takes to find a locally optimal solution. The cost function to minimize for the end-to-end simulation is set equal to the negative of the sum of the post-landing DE+AE stack mass and post-NRI AE mass. The selection of this cost function ensures that the DE and AE payload mass is maximized for the descent and ascent leg, respectively.

The in-space trajectories of the mission implemented in Copernicus consist of the two transfers between the NRHO and LLO (outbound and inbound to the NRHO) and three complete revs along with a phasing rev in LLO prior the DOI burn and following the LLO circularization burn for aligning the perilune of the transfer descent and ascent orbits with the landing site at the time of landing and surface launch, respectively. The six in-space burns are modeled as impulsive burns that connect these in-space trajectory segments. These impulsive burns in the chronological order are: NRD, LOI, DOI, LLO circ., LOD, NRI. The DOI and LLO circ. burns are executed using the reaction control system (RCS) of DE and AE, respectively and the rest are executed by their respective main propulsion systems (MPS). Table 1 gives the maximum thrust available and $I_{sp}$ values of MPS and RCS assumed in this work. Table 2 lists all the control (or optimization) variables and constraints used for the in-space trajectory segments in Copernicus. Near the perilune of the post-DOI descent orbit, the powered descent is initiated to land the DE+AE stack on the lunar surface. After the lunar surface operations, AE launches from the surface and inserts itself into the elliptical ascent orbit (having the same shape as the descent orbit) near its perilune point after

**Table 3. Controls and Constraints for the Powered Descent Segments in Copernicus**

| Controls | Constraints |
|---|---|
| PDI time | DE MPS Thrust $> 20\%$ for all the phases |
| BP duration and throttle | Max LVLH pitch rate = 5 deg/s |
| BP in-plane steering | Max LVLH pitch angular acceleration = 1 deg/s$^2$ |
| AP thrust acceleration | AP starts at a range of $< 2$ km from the landing site |
| AP in-plane steering | Look angle during AP $> 25^\circ$ |
| AP out-of-plane steering | AP time duration $> 45$ s |
| BN duration | BN phase pitch from the vertical $< 32^\circ$ |
| BN thrust acceleration | TD starts at 200 m above the landing site |
| BN in-plane steering | TD initial descent rate = 15 m/s |
| Pitch-up to vertical phase duration | TD descent rate = 1 m/s at 10 m altitude |
| Pitch-up to vertical thrust acceleration | Constant 1 m/s descent rate from 10 m to 1 m altitude |
| Pitch-up to vertical in-plane steering | 5 min $<$ Powered descent duration $<$ 20 min |
| TD phase duration | |
| TD phase thrust acceleration | |

MECO.

The powered descent and ascent trajectories in Copernicus are simulated in the 3-DOF mode, however, the pitch and yaw angles of the vehicle can be determined from the thrust direction. In the nominal design of this mission, the powered descent and ascent trajectories are co-planar with the orbital planes of the descent and ascent LLO, respectively. In other words, DE and AE do not use yaw or out-of-plane steering during the powered descent and ascent except for a very small time duration during the approach and pitch-over phases, respectively. For the pitch angle of DE and AE, the angular rate and acceleration are assumed to be less than 5 deg/s and 1 deg/s$^2$ in Copernicus, respectively. Tables 3 and 4 list all the control variables and constraints used for the powered descent and ascent simulations in Copernicus.

For the end-to-end optimization, the in-space, powered descent, and ascent trajectories of the mission are jointly optimized in Copernicus using its SNOPT solver. SNOPT finds the locally optimal values of all the control variables starting from the initial guesses provided by the analytical solutions such that all the specified constraints are satisfied and the cost function is minimized. The convergence of SNOPT to the desired solution is accelerated because of availability of the close initial guesses for all the control variables from the analytical approximations of the in-space, powered descent, and ascent trajectory segments as discussed earlier. SNOPT refines these initial guesses to find a locally optimal solution in high-fidelity dynamic model that satisfies all the constraints. The entire process for performing end-to-end optimization of the integrated simulation is carried

**Table 4. Controls and Constraints for the Powered Ascent Segments in Copernicus**

| Controls | Constraints |
|---|---|
| Vertical lift-off duration and throttle | Altitude=100 m at the end of vertical lift-off |
| Pitch-over phase duration | Max LVLH pitch rate = 5 deg/s |
| Pitch-over phase velocity azimuth | Max LVLH pitch angular acceleration = 1 deg/s$^2$ |
| Pitch-over phase in-plane steering | Insertion into the ascent orbit at the end of the ascent phase |
| Pitch-over phase out-of-plane steering | Powered ascent total duration $<$ 9 min |
| Ascent phase duration and throttle | |
| Ascent phase in-plane steering | |
| Coast duration in the ascent orbit | |

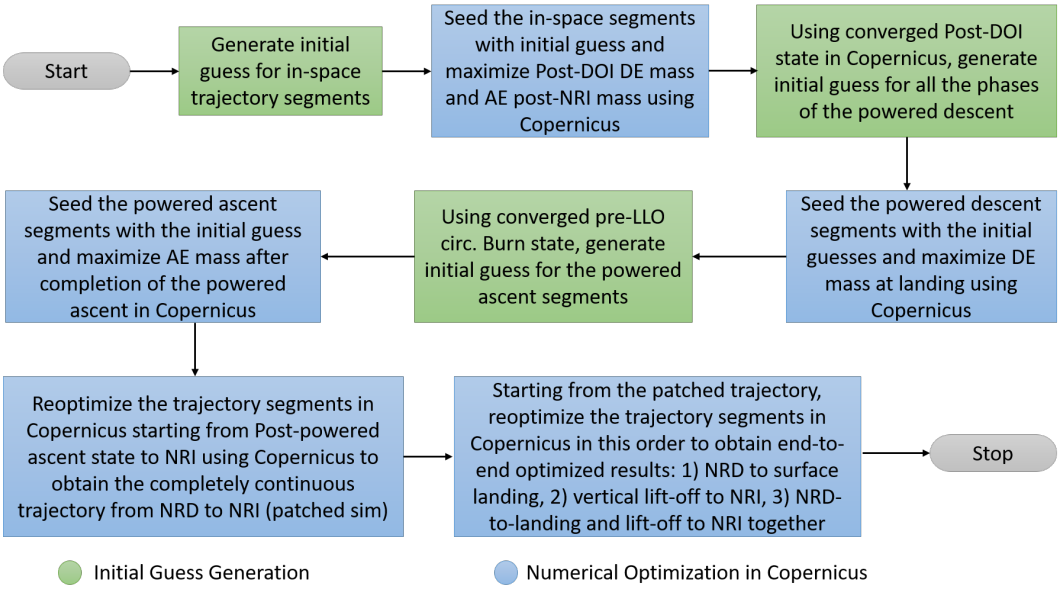


**Figure 6. End-to-End Trajectory Optimization Process using Copernicus and the Analytical Initial Guess Generator for the Lunar Landing Mission**

out in multiple steps in this work and this process is shown in Fig. 6. It is remarked that in the proposed approach for the end-to-end optimization, the in-space and powered-flight trajectories are first optimized separately starting from the analytical approximations and then patched together at the PDI state of DE+AE stack and MECO state of AE. This patched solution is then further optimized in Copernicus by including all the control variables and constraints corresponding to the in-space and powered-flight segments in a single optimization problem. This last step adds an extra degree of freedom in the end-to-end optimization problem in the form of free PDI and MECO states that SNOPT can take advantage of for minimizing the total cost function.

## Results

An example crewed lunar mission that departs from the NRHO on Jan 12, 2025 and lands at a site with latitude and longitude as $-84.17^\circ$ and $59.80^\circ$, respectively, is simulated to validate the performance of the proposed end-to-end optimization approach over the patched trajectory simulation. Two different mission configurations are used: the first one uses the optimizer (SNOPT in this case) to find an optimal surface stay duration (less than the NRHO period of 6.55 days) on the Moon, whereas the second one uses a fixed value for the same that is set equal to the optimal value from the former case plus six hours. For both configurations, SNOPT maximizes the sum of DE+AE stack mass landed at the lunar surface and post-NRI AE mass starting from the analytical initial guesses provided for the control variables. Figures 7 and 8 show the powered descent and ascent trajectory solutions, respectively, computed by the patched (Pat) and end-to-end optimization (Int) approaches with the lunar surface stay duration optimized. It is seen that the powered ascent trajectory computed by the end-to-end optimization approach is close to that of the patched approach. However, PDI in case of the former approach occurs at a lower altitude than the patched approach as seen in the altitude plot in Fig. 7 and as a result, the former solution saves 36 kg of propellant mass when compared to the latter as seen in Table 5. It is noted that in Table 5, the values in column

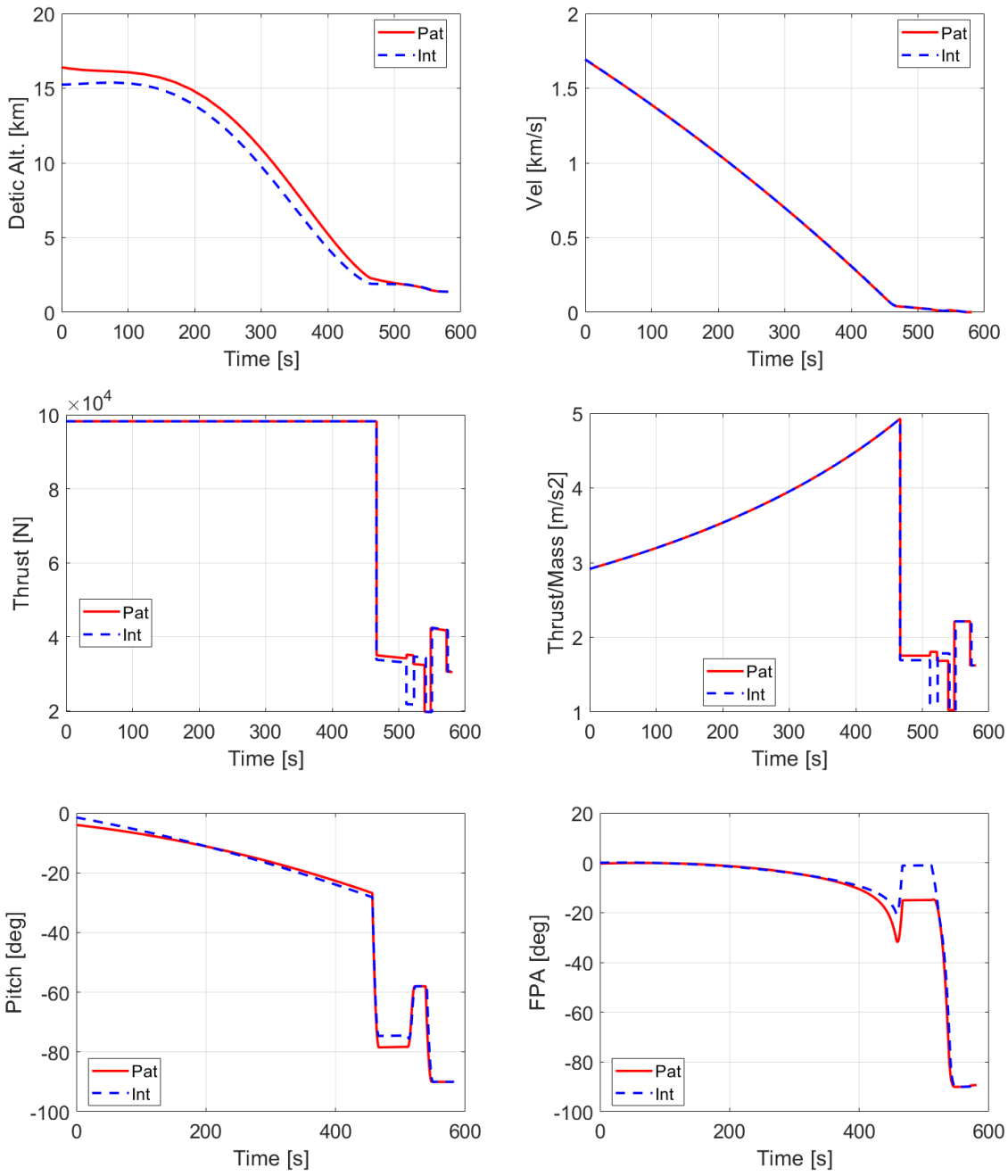


**Figure 7. Powered Descent Trajectory Solutions from the Patched (Pat) and End-to-End Optimized (Int) Trajectory Simulations with Optimal Surface Stay Duration**

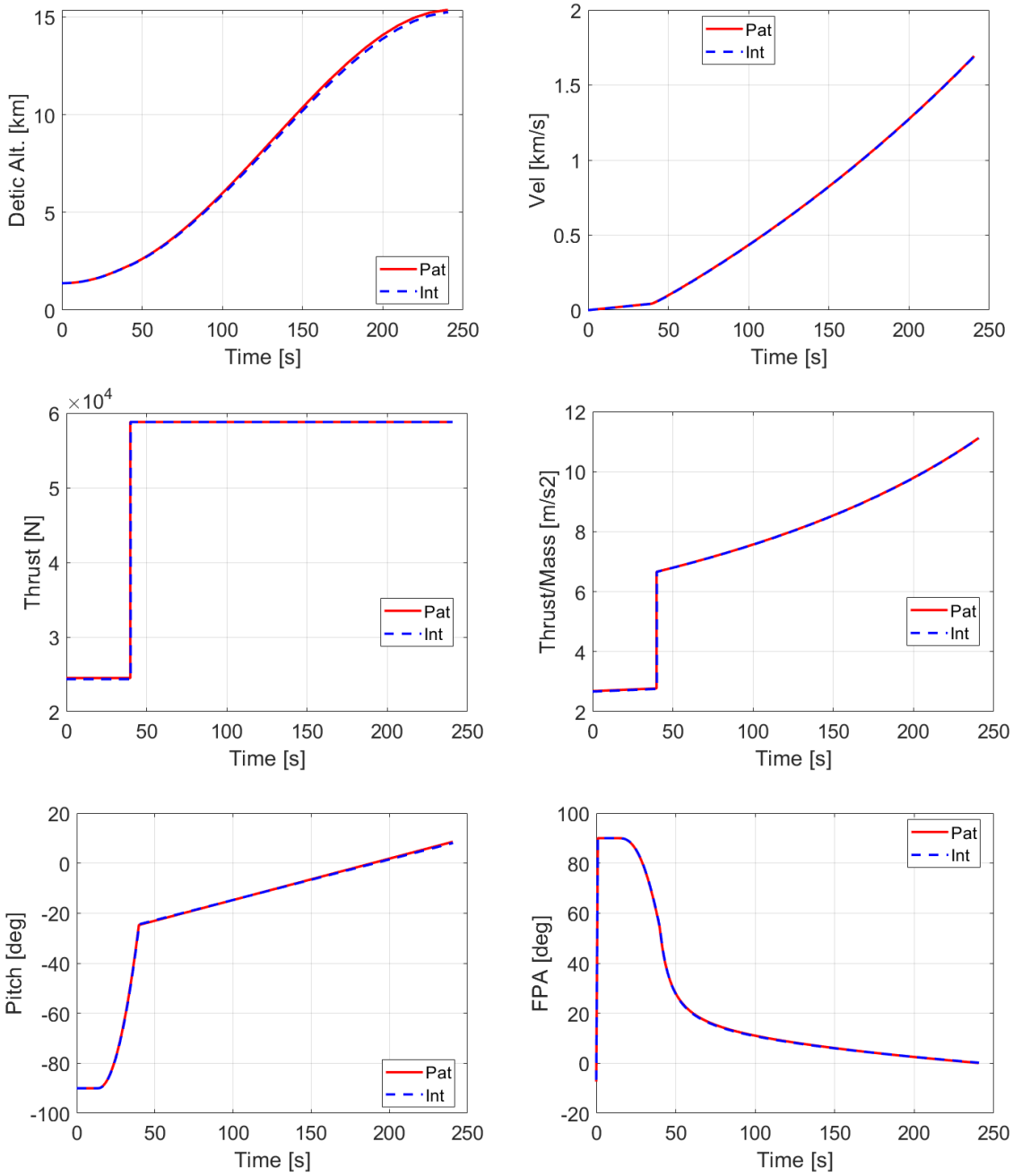


**Figure 8. Powered Ascent Trajectory Solutions from the Patched (Pat) and End-to-End Optimized (Int) Trajectory Simulations with Optimal Surface Stay Duration**

**Table 5. Performance Comparison of Patched and End-to-End Optimized Integrated Mission**

| | Patched Sim (Baseline case) | Integrated Sim | Patched with +6 hr surface stay | Integrated with +6 hr surface stay |
|---|---|---|---|---|
| NRHO-to-LLO $\Delta v$ [m/s] | **734.91** | -0.01 | +0.46 | +1.38 |
| NRHO-to-LLO prop mass [kg] | **8360.86** | -0.09 | +4.70 | +14.05 |
| DOI $\Delta v$ [m/s] | **19.87** | 0 | 0 | 0 |
| PD $\Delta v$ [m/s] | **1952.03** | -6.54 | +6.90 | -6.52 |
| PD prop mass [kg] | **14924.08** | -36.72 | +36.70 | -42.79 |
| PA $\Delta v$ [m/s] | **1817.17** | -0.80 | +54.89 | -0.41 |
| PA prop mass [kg] | **3832.25** | -1.14 | +86.35 | -0.65 |
| LLO circ. burn $\Delta v$ [m/s] | **19.87** | +0.13 | 0 | +0.13 |
| LLO-to-NRHO $\Delta v$ [m/s] | **713.33** | 0 | +346.15 | +340.35 |
| LLO-to-NRHO prop mass [kg] | **1011.77** | +0.22 | +394.89 | +411.76 |
| Total $\Delta v$ [m/s] | **3770.69** | -7.22 | +408.40 | +334.93 |
| Total prop mass used [kg] | **28392.83** | -37.73 | +522.64 | +382.37 |

**Table 6. Timeline Comparison of Patched and End-to-End Optimized Integrated Mission**

| | Patched Sim (Baseline case) | Integrated Sim | Patched with +6 hr surface stay | Integrated with +6 hr surface stay |
|---|---|---|---|---|
| NRD time [hours] | **-12.35** | +0.01 | -0.13 | -0.23 |
| DOI time [hours] | **7.47** | -0.07 | -0.13 | -0.30 |
| PDI time [hours] | **8.34** | 0 | -0.13 | -0.23 |
| PD time duration [min] | **9.68** | +0.03 | +0.05 | +0.03 |
| Surface stay duration [hours] | **141.29** | 0 | +6.13 | +6.13 |
| Lift-off time [hours] | **149.80** | 0 | +6.00 | +5.90 |
| PA time duration [min] | **4.01** | 0 | -0.31 | +0.01 |
| LLO circ. burn time [hours] | **150.79** | -0.02 | +6.00 | +5.87 |
| LOD time [hours] | **158.59** | 0 | +6.09 | +5.80 |
| NRI time [hours] | **170.59** | 0 | +6.09 | +6.00 |
| NRD-to-NRI duration [hours] | **182.94** | 0 | +6.23 | +6.23 |

3 and onward represent the differences from the corresponding baseline values in column 2. Table 6 compares the event timelines of the patched and end-to-end optimized trajectory solutions. The time values in the table corresponding to the baseline case (patched sim) represent the event times measured from the staging vehicle's perilune passing time. It should be noted that PDI and surface lift-off do not occur at the same time in the patched and integrated simulations.

For the configuration with fixed lunar surface stay duration, the end-to-end optimization approach is able to find more efficient powered descent and ascent solutions compared to those of the patched approach as seen in Figs. 9 and 10. The mission performance for the patched and end-to-end optimization approaches are given in columns 3 and 4 of Table 5, respectively. The data shows that the patched solution for this configuration requires an additional 522 kg of propellant compared to only 382 kg for the end-to-end optimized solution over the baseline values. The event timeline comparison (see columns 3 and 4) in Table 6 shows that the end-to-end optimization approach computed the powered ascent solution that is longer in duration by 19 s and as a result, uses 87 kg of less propellant mass when compared to the same computed by the patched approach.

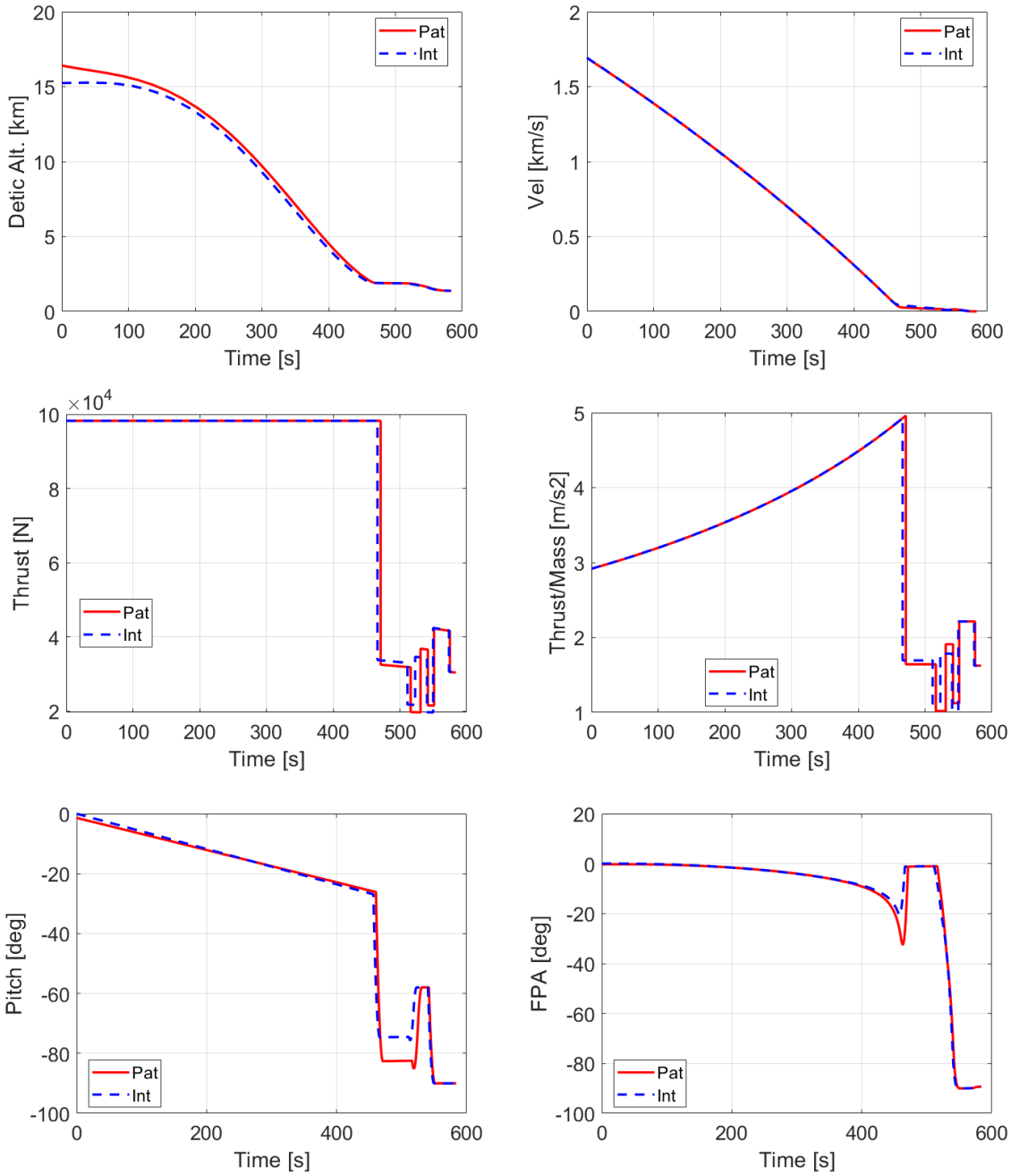


**Figure 9. Powered Descent Trajectory Solutions from the Patched (Pat) and End-to-End Optimized (Int) Trajectory Simulations with Fixed Surface Stay Duration**

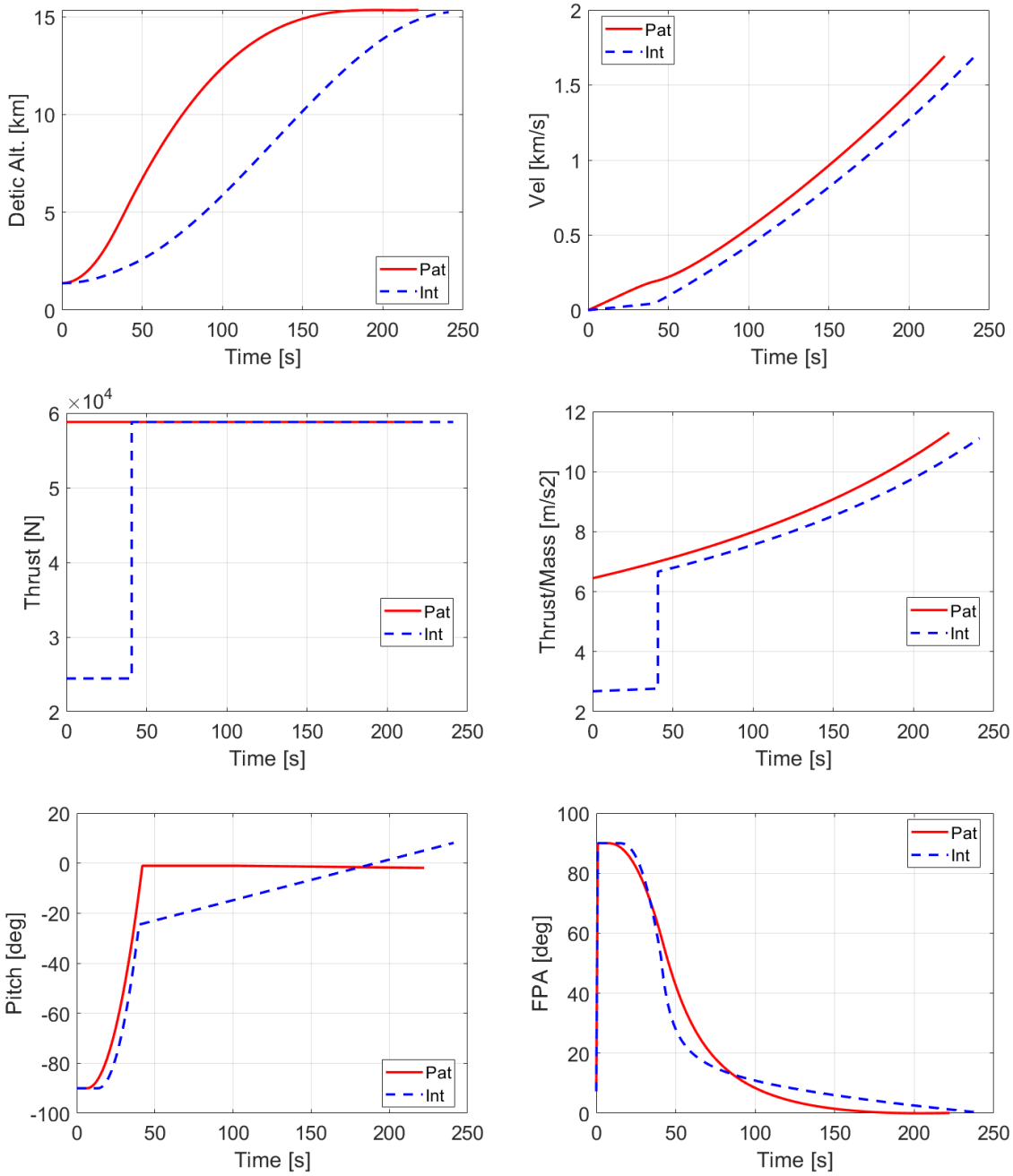


**Figure 10. Powered Ascent Trajectory Solutions from the Patched (Pat) and End-to-End Optimized (Int) Trajectory Simulations with Fixed Surface Stay Duration**

## CONCLUSION

A new integrated approach that is capable of performing end-to-end optimization of a NRHO-staged lunar landing mission, is presented. The proposed approach augments the capability of numerical optimization methods with analytical approximations of the in-space and powered flight segments to avoid the numerical convergence issues. Specifically, new analytical solutions for different phases of the powered descent and ascent trajectory segments are derived that provide close initial guesses for an integrated simulation of the entire mission, from the NRHO departure to the NRHO insertion, in Copernicus trajectory optimization tool. The end-to-end optimization of an example lunar landing mission using the proposed approach showed savings in the propellant mass used when compared to the results obtained using the conventional patched trajectory approach that optimizes the in-space and powered flight segments separately. The proposed integrated simulation is not only useful for performing end-to-end optimization, but it also provides a fast tool for performing trajectory scans for a range of mission epochs and different landing sites. This integrated simulation with in-space and powered flight segments can also be potentially useful in the future for tweaking the nominal mission design to satisfy additional operational constraints such as abort performance or suitable lighting conditions during powered descent.

## ACKNOWLEDGMENTS

The authors would like to acknowledge Cesar A. Ocampo for providing an initial implementation of the in-space trajectories in Copernicus and for reviewing this manuscript. The authors would also like to thank Zachary D. May for providing a POST2-optimized powered descent trajectory for verification and comparison with the powered descent results presented in this work.

## REFERENCES

[1] G. L. Condon, C. C. Esty, C. F. Berry, S. P. Downs, C. Ocampo, B. Mahajan, and L. M. Burke, "Mission and trajectory design considerations for a human lunar mission originating from a near rectilinear halo orbit," *AIAA Scitech 2020 Forum*, 2020, 10.2514/6.2020-1921.

[2] D. Lee, "White Paper: Gateway Destination Orbit Model: A Continuous 15 Year NRHO Reference Trajectory," tech. rep., NASA, 2019.

[3] R. Whitley, J. Gutkowski, S. Craig, T. Dawn, J. Williams, C. Ocampo, W. B. Stein, D. Litton, R. Lugo, and M. Qu, "Combining simulation tools for end-to-end trajectory optimization," *Advances in the Astronautical Sciences*, Vol. 156, 2016, pp. 2811–2826.

[4] R. Lugo, D. Litton, M. Qu, J. Shidner, and R. Powell, "A robust method to integrate end-to-end mission architecture optimization tools," *IEEE Aerospace Conference Proceedings*, Vol. 2016-June, 2016, 10.1109/AERO.2016.7500621.

[5] S. Striepe, "Program to Optimize Simulated Trajectories (POST2), Vol. 2: Utilization Manual, Ver 3.0," tech. rep., NESC, NASA Langley Research Center, 2014.

[6] C. Ocampo, J. S. Senent, and J. Williams, "Theoretical Foundation of Copernicus : a Unified System for Trajectory Design and Optimization," *4th International Conference on Astrodynamics Tools and Techniques*, 2010.

[7] K. D. Hicks, "Introduction to Astrodynamic Re-Entry," *Introduction to Astrodynamic Re-Entry*, 2007, pp. 321–356.

[8] R. K. Cheng, C. M. Meredith, and D. A. Conrad, "Design considerations for surveyor guidance," *Journal of Spacecraft and Rockets*, Vol. 3, No. 11, 1966, pp. 1569–1576, 10.2514/3.28709.

[9] C. R. McInnes, "Gravity-turn descent from low circular orbit conditions," *Journal of Guidance, Control, and Dynamics*, Vol. 26, No. 1, 2003, pp. 183–185, 10.2514/2.5033.

[10] P. Lu and S. A. Sandoval, "Abort Guidance during Powered Descent for Crewed Lunar Missions," No. January, 2021, pp. 1–15, 10.2514/6.2021-0505.

[11] J. S. Meditch, "On the Problem of Optimal Thrust Programming For a Lunar Soft Landing," *IEEE Transactions on Automatic Control*, Vol. 9, No. 4, 1964, pp. 477–484, 10.1109/TAC.1964.1105758.